Statistical Properties of Quasi-periodic Electromagnetic Ion Cyclotron Waves: ULF Modulation Effects

Muhammad Shahid[1,2], M. Fraz Bashir[2], A. V. Artemyev[2,3], X.-J. Zhang [4,2], Vassilis Angelopoulos[2], G. Murtaza [1]

[1]Salam Chair in Physics, Government College University Lahore, Pakistan
[2]Department of Earth, Planetary, and Space Sciences, University of California, Los Angeles, USA
[3]Space Research Institute, Russian Academy of Sciences, Moscow, Russia
[4]Department of Physics, University of Texas at Dallas, Richardson, TX, USA

Key Points:

- We conduct statistics of quasi-periodic EMIC waves modulated by compressional ULF waves
- Most ULF-modulated EMIC waves are observed on dayside magnetosphere at $L \in [8, 12]$
- We construct an empirical model for EMIC wave characteristics as a function of L-shell and MLT

Corresponding author: Muhammad Shahid, `shahidm689@yahoo.com`

Abstract

Electromagnetic ion cyclotron (EMIC) waves effectively scatter relativistic electrons in the Earth's radiation belts and energetic ions in the ring current. Empirical models parameterizing EMIC wave characteristics are important elements of inner magnetosphere simulations. Two main EMIC wave populations included in such simulations are the population generated by plasma sheet injections and another population generated by magnetospheric compression due to solar wind. In this study, we investigate a third class of EMIC waves, generated by hot plasma sheet ions modulated by compressional ultra-low-frequency (ULF) waves. Such ULF-modulated EMIC waves are mostly observed on the dayside, between magnetopause and the outer radiation belt edge. We show that ULF-modulated EMIC waves are weakly oblique (with wave normal angle $\approx 20^\circ \pm 10^\circ$) and narrow banded (with spectral width of $\sim 1/3$ of the mean frequency). We further construct an empirical model of EMIC wave characteristics as a function of L-shell and MLT. The low ratio of plasma frequency to electron gyrofrequency ($f_{pe}/f_{ce} \sim 5-10$) around the EMIC wave generation region does not allow these waves to scatter energetic electrons. However, these waves provide very effective (comparable to strong diffusion) quasi-periodic precipitation of plasma sheet protons.

1 Introduction

Electromagnetic ion cyclotron (EMIC) waves are the primary wave mode responsible for scattering and heating of cold ions (e.g., Kitamura et al., 2018; Ma et al., 2019) and precipitating relativistic electrons in the inner magnetosphere (see, e.g., Millan & Thorne, 2007; Usanova et al., 2014; Yahnin et al., 2017; Drozdov et al., 2022; Bashir et al., 2022; Angelopoulos et al., 2023, and references therein). These waves can be generated by hot, transversely anisotropic ions injected from the plasma sheet and drifting duskward (e.g., L. Chen et al., 2010; Jun et al., 2019; Bashir et al., 2022, and references therein). Such a localized EMIC generation region leads to the prevalence of EMIC-driven relativistic electron precipitation at the nightside/dusk flank (e.g., Blum et al., 2015; Yahnin et al., 2016; Capannolo et al., 2019, 2023). EMIC waves can also be generated by another mechanism on the dayside. This mechanism involves intense, compressional ultra-low-frequency (ULF) waves that may magnetically trap anisotropic, hot ion populations and transport them into the inner magnetosphere. Such ULF waves are often generated in response to the magnetopause impact by solar wind/magnetosheath transients (e.g., M. D. Hartinger et al., 2013, 2014; Wang et al., 2018; Wang, Nishimura, et al., 2019). Another ULF mode capable of hot ion trapping and transport is the drift mirror mode (e.g., Hasegawa, 1969): nonlinear mirror mode waves are local magnetic field depletions filled with transversely anisotropic hot ions (Rae et al., 2007; Balikhin et al., 2009; Soto-Chavez et al., 2019; Cooper et al., 2021). Nonlinear mirror waves are generated around the magnetopause and can transport trapped ion population earthward (due to convection electric field), where larger cold background density change the stability conditions of this population and may drive EMIC wave generation within mirror modes (Loto'Aniu et al., 2009; Kitamura et al., 2021; Z. Y. Liu et al., 2022; Yin et al., 2022).

In contrast to EMIC waves generated by plasma sheet ion injections (e.g., Jun et al., 2019, 2021) and thus parameterized by geomagnetic indexes and solar wind conditions (e.g., Usanova et al., 2012; Ma et al., 2015; H. Chen et al., 2019; Ross et al., 2021; Gamayunov et al., 2020), the ULF-associated EMIC waves are not expected to strongly correlate with geomagnetic conditions; instead, they should be mostly determined by dayside magnetosphere interaction with mesoscale (or even ion kinetic scale) transients. Thus, this EMIC wave population may be smoothed out in an index-based empirical model and requires alternative parameterization for further incorporation into simulations of the radiation belt dynamics in the inner magnetosphere. Such ULF-associated EMIC waves may play an important role in relativistic electron precipitation at higher L-shells, well outside the plasmapause (see statistics of relativistic electron precipitation events at high-L in Capannolo et al., 2022). Moreover, the small scale of mirror mode structures (the primary source of ULF-modulated EMIC waves), relative to the usually large-scale EMIC wave generation region (Blum et al., 2016, 2017) may explain the temporally and spatially localized EMIC-driven electron precipitation in observations (Shumko et al., 2022). Additionally, EMIC waves are also responsible for scattering and isotropization/precipitation of ring current ions (e.g., Jordanova et al., 2001, 2007; Khazanov et al., 2007). Therefore, EMIC wave modulation/generation within mirror mode structures indicates the solar wind impact on ring current dynamics.

This study aims to statistically investigate the characteristics of ULF-modulated EMIC waves, their spatial (in L-shell, MLT) distribution, and the associated plasma conditions. We utilize 5 years (2017-2021) of THEMIS E (Angelopoulos, 2008) measurements in the inner magnetosphere and near-Earth plasma sheet. The collected dataset contains 330 intervals with multiple EMIC bursts modulated by compressional ULF waves, with a total of 1555 individual bursts (each of them is within $\sim 1/2$ period of the simultaneously observed ULF wave). Section 2 describes typical events from our dataset, whereas Section 3 provides statistical properties of EMIC waves and surrounding plasma characteristics. The results are discussed and concluded in Section 4.

2 Spacecraft Instruments and Dataset

We examine data from three inner probes of THEMIS mission at an apogee of $\sim$ 12 Earth radii (RE). These probes are equipped with identical instruments (Angelopoulos, 2008), and for investigation of EMIC waves we use: Fast Survey (1/4s sampling) measurements of the fluxgate magnetometer (FGM, see Auster et al., 2008), spin averaged (3s) measurements of ion and electron $<$ 30keV spectra and moments by the electrostatic analyzer (ESA, see McFadden et al., 2008), cold plasma density derived from the spacecraft potential (Bonnell et al., 2008; Nishimura et al., 2013). Ion temperature has been derived from combined measurements of ESA and solid state telescope (SST, see Angelopoulos et al., 2008). Our event selection criteria include: (1) search for quasi-periodic EMIC waves with at least three wave intensity peaks within one hour, (2) determine the ULF wave frequency range (within $[2.5, 20]$ mHz) exhibiting good correlation between ULF magnetic field minima and EMIC intensity peaks. Only events exhibiting such correlations are included in the dataset.

Figure 1 shows three typical events from the collected dataset. All are from the near-equatorial (B_z is the dominant component; see Panel (a)) transition region between the plasma sheet and the inner magnetosphere. The plasma frequency to electron gyrofrequency ratio, $f_{pe}/f_{ce} \in [5, 10]$, is typical for the near-Earth plasma sheet (see Panel (b)). Note that f_{pe}/f_{ce} derived from the spacecraft-potential density is much larger than f_{pe}/f_{ce} based on ESA density measurements, because a significant fraction of cold electrons are not measured by the ESA (McFadden et al., 2008).

Using magnetic field measurements, $\mathbf{B}$, we evaluate compressional fluctuations in the ULF frequency range: $\delta B_\parallel = (\mathbf{B} - \langle\mathbf{B}\rangle)\cdot\langle\mathbf{B}\rangle/|\langle\mathbf{B}\rangle|$. Panels (c) show quasi-periodic $\delta B_\parallel$ variations with amplitudes of a fraction of nT, i.e., $\delta B_\parallel/|\langle\mathbf{B}\rangle| \sim 10^{-3}$. To evaluate $\delta B_\parallel$, we use the frequency range $[2.5, 20]$ mHz (i.e., $\langle...\rangle$ denotes 7 min averaging). For each event, we additionally check if changing the lower and upper-frequency limits (within the $[2.5, 20]$ mHz range) may improve the $\delta B_\parallel$ correlation with EMIC wave intensity, and adjust these limits to maximize this correlation.

Such compressional ULF waves propagate in a hot, transversely anisotropic ion background (see Panels (d,e)), despite the low amplitude, can drive EMIC wave generation. Panels (f) show quasi-periodic EMIC bursts correlated with local minima of $\delta B_\parallel$, which are usually associated with enhanced hot transversely anisotropic ion population contributing to the pressure balance (e.g., Balikhin et al., 2009; Soto-Chavez et al., 2019). Wave ellipticity and polarization (panels (g,h)) confirm that these are classical, field-aligned EMIC waves.

Figure 2 zooms in several EMIC bursts from Fig. 1. All bursts are associated with local minima of ULF $\delta B_\parallel$, and such type of correlation has been found for all events in our dataset. Root mean square wave amplitude $\langle B_w\rangle = \left(\int_{f_{cp}/4}^{f_{cp}} B_w^2(f)df\right)^{1/2}$ is about $0.2-1$nT and mean wave frequency $\langle f\rangle = \int_{f_{cp}/4}^{f_{cp}} fB_w^2(f)df/\langle B_w\rangle^2$ is about $0.2-0.4f_{cp}$, quite typical for EMIC waves in the inner magnetosphere (see, e.g., Kersten et al., 2014; Zhang et al., 2016). For each wave burst, we also calculate wave frequency width $df = \int_{f_{cp}/4}^{f_{cp}}(f-\langle f\rangle)^2\mathcal{B}_w^2(f)df/\langle B_w\rangle^2$, mean wave normal angle WNA, and the dispersion of wave normal angles, $dWNA$. Wave bursts shown in Fig. 2 are quite narrow-banded with $df/\langle f\rangle < 1/5$ and weakly oblique with $WNA \approx 20^\circ \pm 10^\circ$. We determine these characteristics for all wave bursts in our dataset.

Figure 3 shows histograms for L-shell and MLT distributions for all datasets: ULF-modulated EMIC waves are mostly observed at high L-shells ($L > 8$) at the dayside sector (from 10 to 16), where compressional ULF waves are predominantly observed in response to solar wind transients and magnetopause oscillations (M. Hartinger et al., 2011; M. D. Hartinger et al., 2013; Wang et al., 2018; Wang, Nishimura, et al., 2019). At dawn

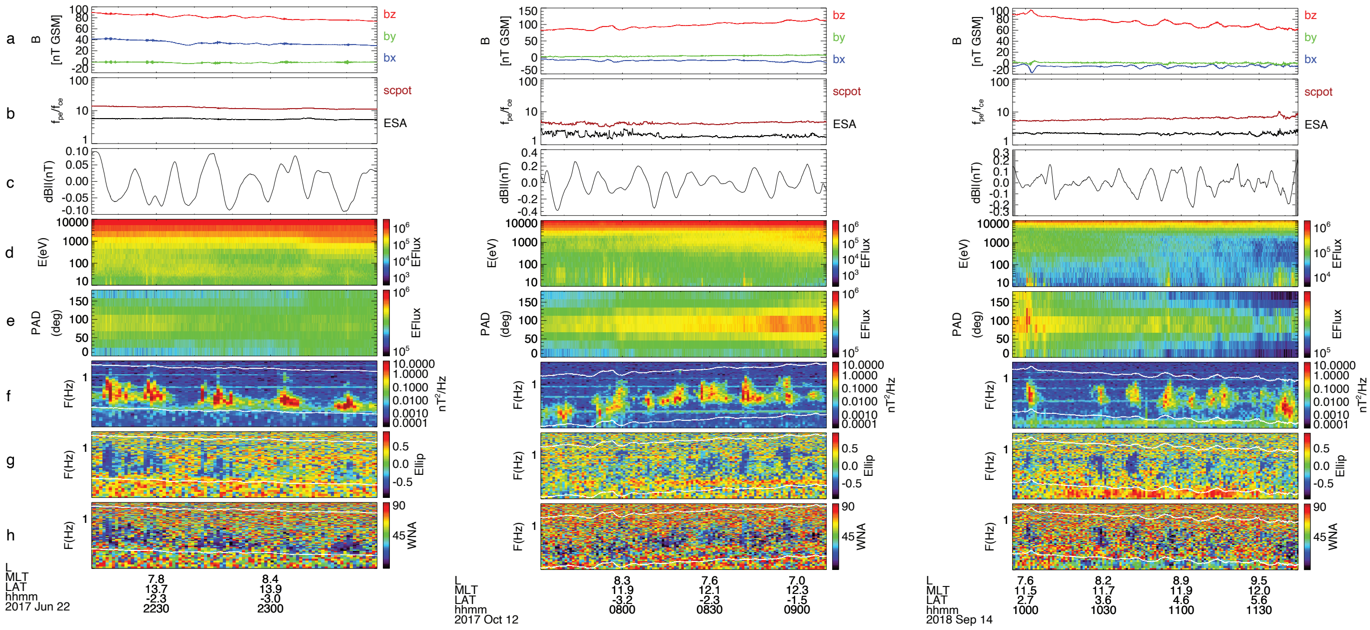

Figure 1. Three example events with quasi-periodic EMIC waves: (a) GSM magnetic field components, (b) f_{pe}/f_{ce} ratio, (c) ULF $\delta B_{\|}$ field, (d) omni-directional spectrum of ions,(e) pitch-angle distribution of ~ 10 keV ions, (f) EMIC wave magnetic field spectrum with main frequencies shown in white, (g) EMIC wave ellipticity, (h) EMIC wave normal angle.

and dusk flanks, ULF-modulated EMIC waves are only observed at high L, whereas at the dayside sector such waves can be found even at $L \sim 5-6$.

3 Statistical properties of ULF-modulated EMIC waves

Figure 4 shows distributions of statistical properties of ULF-modulated EMIC waves. Burst-averaged wave amplitude (square root of the average wave intensity) is usually within $[50, 500]$pT, but there are rare observations of very intense ($\sim$ 1nT) waves (see panel (a)). These are typical intensities of the inner magnetosphere EMIC waves (Zhang et al., 2016; Jun et al., 2019). Most waves are observed in quite rarefied plasma environment with $f_{pe}/f_{ce} < 10$ (see panel (b)), typical in the plasma sheet, but much smaller than f_{pe}/f_{ce} in plasmaspheric density plumes (typical generation region of EMIC waves Usanova et al., 2013; Halford et al., 2015). As f_{pe}/f_{ce} controls the electron resonant energies for EMIC waves, small $f_{pe}/f_{ce} < 10$ would not allow EMIC waves to scatter $\leq$ 1 MeV electrons (Summers & Thorne, 2003), and only a small population of observations with $f_{pe}/f_{ce} > 15$ can explain the ≤ 1 MeV electron precipitation.

Most ULF-modulated EMIC waves are moderately oblique with $WNA \in [30^\circ, 60^\circ]$, with quite a small variation of wave normal angle, $dWNA \sim 7^\circ$ (see panels (c,d)). Such obliqueness may affect relativistic electron scattering by EMIC waves (Khazanov & Gamayunov, 2007; Gamayunov & Khazanov, 2007) and should be quite important for EMIC wave Landau resonance with warm electrons (Fu et al., 2018; Wang, Li, et al., 2019; Inaba et al., 2021) and plasma sheet ions (Ma et al., 2019; Usanova, 2021). The observed ULF-modulated EMIC wave frequencies and the frequency widths, $\langle f \rangle / f_{ce} \in [0.4, 0.55]$ and $\Delta f / f_{cp} \in [0.1, 0.2]$ (see panels (e,f)), are typical for EMICs in the inner magnetosphere (Kersten et al., 2014; Zhang et al., 2016).

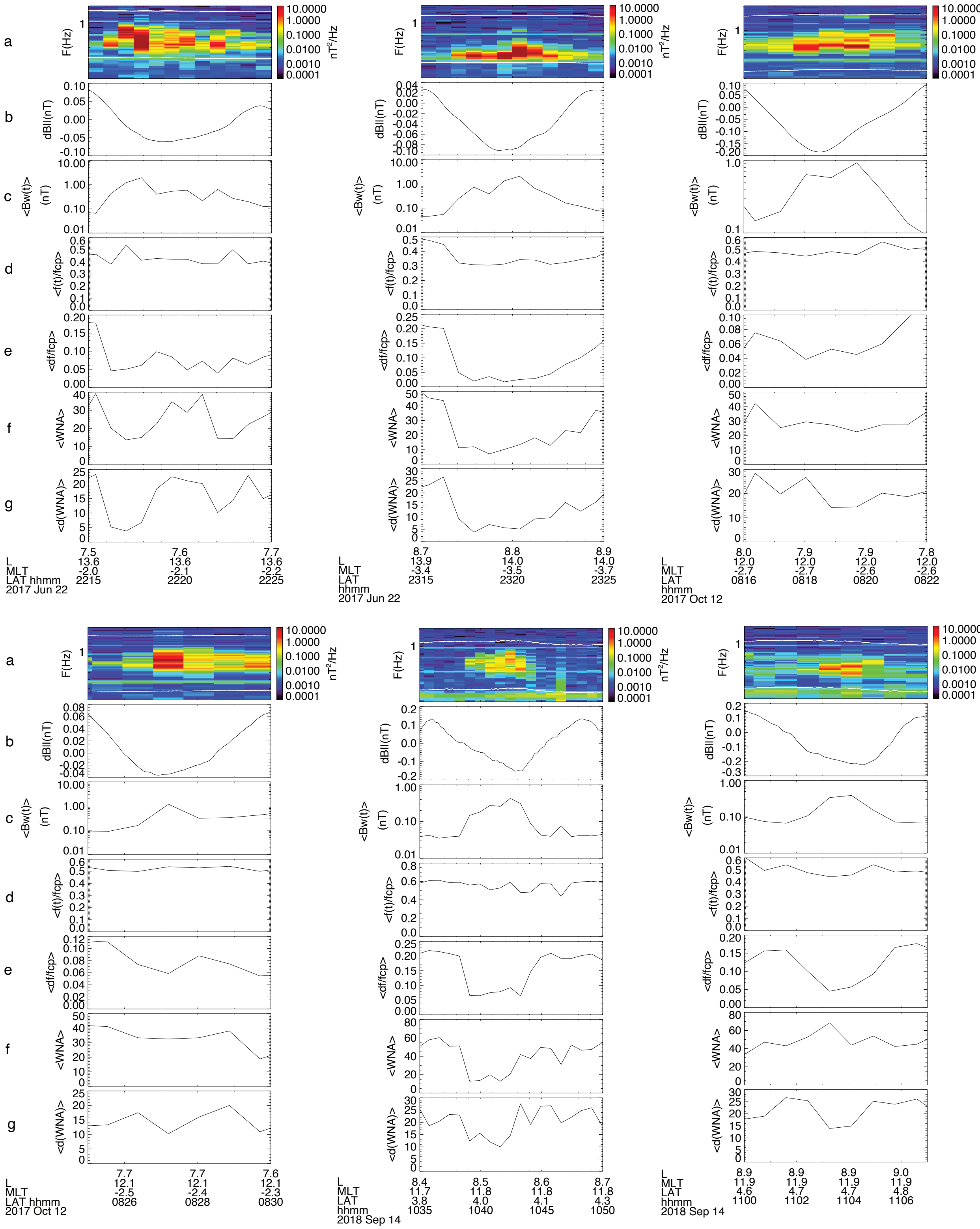

Figure 2. Characteristics of individual EMIC wave bursts associated with local $\delta B_{\parallel}$ minima for three events from Fig. 1:(a) EMIC wave intensity $\langle B_w^2 \rangle$, (b) ULF field minima, (c) EMIC wave amplitude, (d) EMIC wave mean frequency normalized to f_{cp}, (e) width of EMIC wave mean frequency normalized to f_{cp}, (f) EMIC wave mean wave normal angle, and (g) width of the wave normal angle distribution.

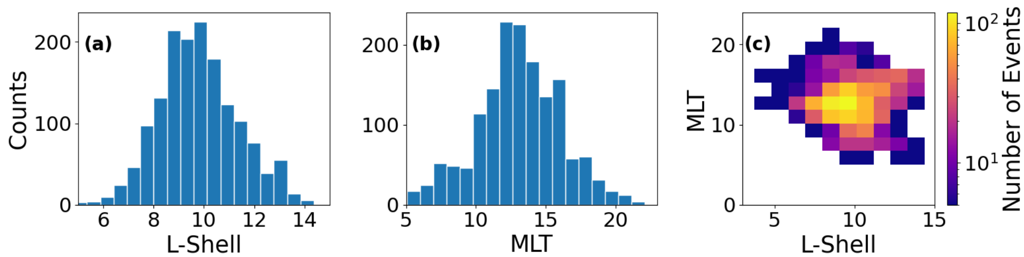

Figure 3. Distribution of events (individual EMIC wave bursts associated with ULF $\delta B_{\|}$ minimum): (a) L-shell distribution, (b) MLT distribution, and (c) distribution of the total number of events in (L, MLT) plane.

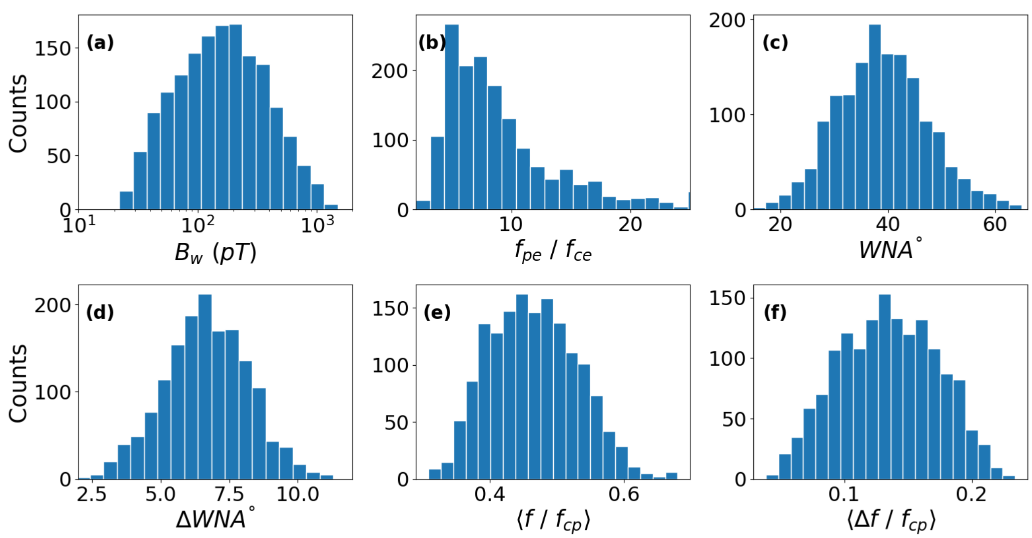

Figure 4. (a) Distributions of EMIC wave amplitudes $\sqrt{\langle B_w^2 \rangle}$, (b) f_{pe}/f_{ce} ratio, (c) mean wave normal angle, (d) width of the wave normal angle distribution, (e) mean wave frequency $\langle f/f_{cp} \rangle$, and (f) wave frequency width $\langle \Delta f/f_{cp} \rangle$.

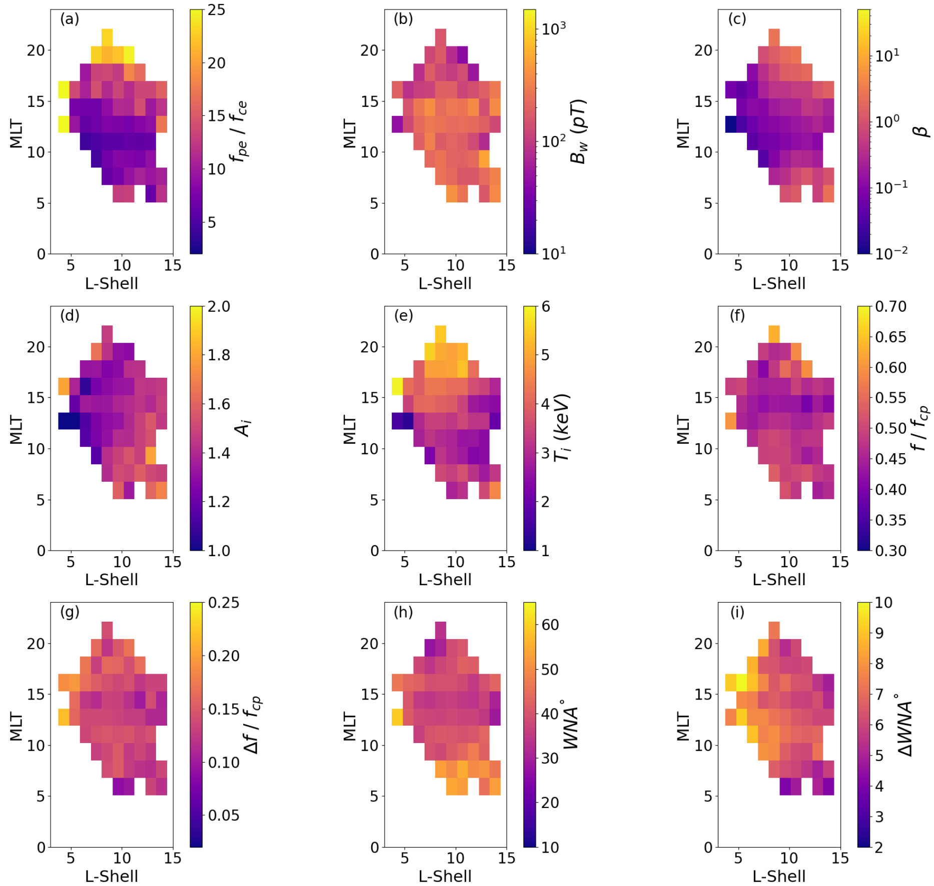

Figure 5. Distributions of main wave characteristics from Fig. 4 in (L, MLT) plane. (a) f_{pe}/f_{ce}, (b) wave amplitude B_w, (c) plasma β_i, (d) temperature anisotropy, (e) ion temperature in keV, (f) normalized wave frequency, (g) normalized width of wave frequency, (h) wave normal angle, (i) width of wave normal angle.

Figure 5 shows the spatial distribution of all wave and background plasma/magnetic field characteristics. There is a clear dawn-dusk asymmetry of f_{pe}/f_{ce} and ion temperature T_i for ULF-modulated EMIC events: f_{pe}/f_{ce} is about 10 at the dawn flank and increases to 20 at the dusk flank; T_i is about 3 keV at the dawn flank and increases to 5keV at the dusk flank. The root mean square amplitude is slightly larger on the dawn flank, $\langle B_w \rangle \sim 200$pT, than on the dusk flank, $\langle B_w \rangle \sim 50$pT. Ion $\beta = 8\pi n T_i / B_0^2$ maximises at flanks, $\beta_i \sim 10$, and has a minimum at dayside and at low L, $\beta_i < 1$. Ion temperature anisotropy, the key parameter for wave generation, has a maximum at dawn flank, $A_i = T_{i,\perp}/T_{i,\parallel} \sim 1.6$. This peak of A_i most likely explains the dawn flank peak of $\langle B_w \rangle$.

Panels (h-l) in Fig. 5 show the distribution of the main wave characteristics. Mean wave frequency $\langle f \rangle / f_{cp}$ and frequency width df/f_{cp} do not vary much with MLT: for example, there is only a slightly lower $\langle f \rangle / f_{cp} \approx 0.4$ at the dusk flank, in comparison with $\langle f \rangle / f_{cp} \approx 0.5$ on the dawn-side. However, there is a clear gradient of wave normal angle with MLT: waves at the dusk flank are more field-aligned with $WNA \approx 35^\circ$ than in the dawn flank, where $WNA \approx 55^\circ$. Interestingly, the wave normal angle variation, $dWNA$, does not depend on MLT, but increases at lower L-shells, from $dWNA \sim 5^\circ$ at $L \sim 12$ to $dWNA \sim 10^\circ$ at $L \sim 5$.

Distributions of the main wave characteristics shown in Fig. 5 can be used to estimate the ion diffusion rates that would describe plasma sheet and ring current ion precipitation via resonant scattering by ULF-modulated EMIC waves. To enable the evaluation of diffusion rates, we fit the normalized wave intensity $(B_w/B_0)^2$, mean wave frequency and frequency distribution width, $\langle f\rangle/f_{cp}$ and $\Delta f/f_{cp}$, and plasma to electron cyclotron frequency ratio, f_{pe}/f_{ce}, as function of MLT and L. We use the following fitting function

$$F = a_0+a_1\cdot(L/10)+a_2\cdot MLT+a_3\cdot(L/10)\cdot MLT+a_4\cdot(L/10)^2\cdot MLT+a_5\cdot(L/10)\cdot MLT^2 \quad (1)$$

that capture main L and MLT gradients of wave characteristics. Note that these fittings only work within the region of ULF-modulated EMIC wave observations: $MLT \in [5, 20]$, $L \in [5, 12]$, with two boundaries $MLT_- = 15-L$ and $MLT_+ = 10+L$. Table 1 shows the coefficients of these fittings.

Parameters	a_0	a_1	a_2	a_3	a_4	a_5
f_{pe}/f_{ce}	-2.32	22.79	0.75	-3.72	0.26	0.13
B_w(pT)	0.26	-0.21	0.01	0.00	0.01	0.00
β	1.22	2.83	-0.05	-0.67	0.07	0.02
A_i	0.67	1.05	0.00	0.03	-0.01	0.00
T_i(keV)	-0.25	5.44	0.03	-0.13	-0.34	0.02
f/f_{cp}	0.94	-0.18	-0.03	0.00	0.00	0.00
$\Delta f/f_{cp}$	0.22	-0.05	0.00	0.00	0.00	0.00
WNA°	67.06	16.19	-1.16	-5.88	0.93	0.19
$dWNA^\circ$	11.83	-8.00	0.06	0.22	0.19	-0.02

Table 1. Coefficients from fitting EMIC wave characteristics, see Eq. (1).

Using these fittings of EMIC wave characteristics, we can quantify the wave contribution to plasma sheet and ring current ion losses. For this reason, we evaluate pitch-angle diffusion rates due to cyclotron-resonant interaction with EMIC waves. We use a simplified formula by assuming the waves as field-aligned, although some of them are weakly oblique (see Summers et al., 2007, for equations of diffusion coefficients in the quasi-linear theory):

$$D_{\alpha\alpha} = \frac{\pi}{2}\frac{1}{c\beta}\frac{\Omega_{cp}^2}{|\Omega_{ce}|}\frac{1}{(E+1)^2}\frac{R(1-\frac{x\cos\alpha}{y\beta})^2|F(x,y)|}{\delta x|\beta\cos\alpha - F(x,y)|}e^{-(\frac{x-x_m}{\delta x})^2}$$

where $x = f/f_{cp}$, $y = kc/2\pi f_{cp}$, E is the dimensionless particle kinetic energy given by $E = E_k/(m_i c^2) = \gamma - 1$, $\beta = [E(E+2)]^{1/2}/(E+1)$, $R = B_w^2/B_0^2$ is the ratio of the energy density of the wave magnetic field to that of the background field, i.e., the relative wave power; $x_m = \langle f\rangle/f_{cp}$, $\delta x = \Delta f/f_{cp}$, and $F(x,y) = dx/dy$ is determined from the cold plasma dispersion of EMIC waves (Stix, 1962). The diffusion rate $D_{\alpha\alpha}$ evaluated at the loss-cone pitch-angle, $\alpha_{LC}(L)$, determines the rate of wave-driven ion precipitation into the atmosphere (Kennel & Petschek, 1966). This diffusion rate can be compared with the so-called strong diffusion rate(Summers & Thorne, 2003)

$$D_{SD} = \frac{9.66}{L^4}\left[\frac{4L}{4L-3}\right]^{1/2}\frac{[E(E+2)]^{1/2}}{(E+1)}$$

that determines the maximum possible precipitation rate in the diffusion regime (Kennel & Petschek, 1966; Kennel, 1969). Figure 6 shows diffusion rates $D_{\alpha\alpha}$ and $D_{\alpha\alpha}/D_{SD}$ at four ion energies and $\alpha_{LC}(L)$. At $MLT \in [5, 15]$ and $L > 10$, ULF-modulated EMIC waves provide very strong $D_{\alpha\alpha} \sim 10^{-3}\mathrm{s}^{-1}$, above the strong diffusion limit ($D_{\alpha\alpha}/D_{SD} >$

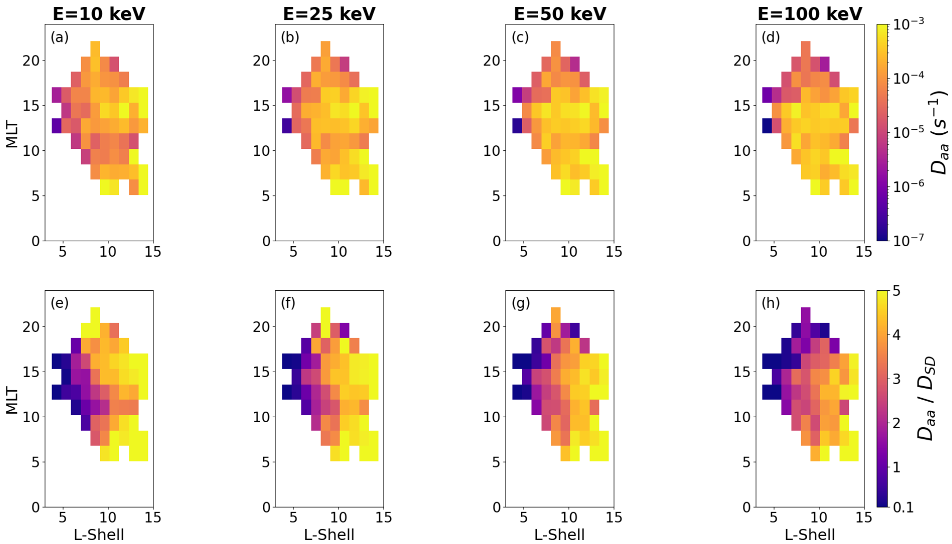

Figure 6. Distribution of pitch-angle diffusion coefficients in (L, MLT) plane at $E = (10, 25, 50, 100)$ keV (a-d) $D_{\alpha\alpha}$ distribution (e-h) $D_{\alpha\alpha}/D_{SD}$ distribution.

1). Thus, when these waves are present (i.e., when sufficiently strong ULF waves transport hot anisotropic ions and EMIC waves), they will drive the modulated ion (proton) losses for a wide energy range. Such losses can be observed as day-side proton aurora forms (e.g., Sigernes et al., 1996; Lorentzen & Moen, 2000; Berchem et al., 2003; Frey, 2007).

4 Discussion and Conclusions

In this study, we examine a specific class of EMIC waves modulated by compressional ULF waves. The likely scenario for such EMIC wave generation includes the day-side magnetopause impact by solar wind transients that drive compressional ULF waves (presumably drift mirror mode waves Rae et al., 2007; Balikhin et al., 2009; Soto-Chavez et al., 2019; Cooper et al., 2021), and these ULF waves transport the hot, transversely anisotropic ion population to lower L-shells, where the ion anisotropy is released in the form of EMIC wave generation (see examples in Loto'Aniu et al., 2009; Kitamura et al., 2021; Z. Y. Liu et al., 2022; Yin et al., 2022). This scenario is confirmed by the prevalence of ULF-modulated EMIC waves at large L-shells ($L \in [8, 12]$) on the day-side $MLT \in [10, 16]$. Therefore, we may suggest that such ULF-modulated EMIC waves constitute an additional class of EMICs, supplementing the two most investigated classes: EMICs generated on the dusk flank by plasma sheet injected ions and EMICs generated at low L-shells on the day-side by compressionally heated ions (e.g., Jun et al., 2019, 2021; N. Liu et al., 2022; Xue et al., 2022). The main feature of this new EMIC wave class is the periodicity of EMIC emission.

These ULF-modulated EMIC waves are moderately oblique ($WNA \in [30°, 60°]$), quite narrow-banded ($\Delta f/f \sim 0.3$ with $f/f_{cp} \in [0.4, 0.55]$), and moderately intense ($B_w \in [50, 300]$pT). Due to their insufficiently-high wave amplitudes, these waves resonate with ions in the quasi-linear regime. The main ion population responsible for ULF-modulated EMIC wave generation is typical plasmasheet ions with energies $E_R \in [5, 15]$keV. Due to the relatively small plasma density at high L, the frequency ratio f_{pe}/f_{ce} during ULF-modulated EMIC waves is about $\in [5, 10]$. This ratio controls the resonant energies for electrons interacting with EMIC waves, and when $f_{pe}/f_{ce} \in [5, 10]$ EMIC waves cannot scatter relativistic or energetic electrons, but only ultra-relativistic electrons that are usually scarce in such high L-shells. Therefore, ULF-modulated EMIC waves are not effective in driving electron losses. However, these waves are very effective in scattering ions (pitch-angle diffusion rate reaches the strong diffusion limit for $[10, 100]$keV ions). Therefore, ULF-modulated EMIC waves can produce quasi-periodic ion precipitation contributing to day-side proton aurora (Sigernes et al., 1996; Lorentzen & Moen, 2000; Berchem et al., 2003; Frey, 2007). Further transported by ULF waves to lower L-shells, hot anisotropic ion population may generate EMICs within the outer radiation belt where these waves is expected to serve as the seed population for intense coherent EMIC waves (see discussions in Gamayunov & Engebretson, 2021, 2022).

Statistics of ULF-modulated EMIC waves demonstrate one more mechanism of direct solar wind impact on the Earth's magnetosphere (see discussions of other mechanisms in M. D. Hartinger et al., 2013, 2014; Wang et al., 2018; Wang, Nishimura, et al., 2019), which underlines the importance of including solar wind transients into models of inner magnetosphere dynamics and magnetosphere-ionosphere coupling.

Acknowledgments

We acknowledge the support of NASA contract NAS5-02099 for the use of data from the THEMIS Mission, specifically K. H.Glassmeier, U. Auster and W. Baumjohann for the use of FGM data (provided under the lead of the Technical University of Braunschweig and with financial support through the German Ministry for Economy and Technology and the German Center for Aviation and Space (DLR) under contract 50 OC 0302). Work of M.F.B., A.A., X.-J. Z. are supported by NSF grant #2329897, and NASA grants #80NSSC20K1270, #80NSSC23K0403, #80NSSC23K0108 .

Open Research

THEMIS data is available at http://themis.ssl.berkeley.edu. Data access and processing was performed using SPEDAS V4.1, see Angelopoulos et al. (2019).

References

Angelopoulos, V. (2008, December). The THEMIS Mission. *Space Sci. Rev.*, *141*, 5-34. doi: 10.1007/s11214-008-9336-1

Angelopoulos, V., Cruce, P., Drozdov, A., Grimes, E. W., Hatzigeorgiu, N., King, D. A., ... Schroeder, P. (2019, January). The Space Physics Environment Data Analysis System (SPEDAS). *Space Sci. Rev.*, *215*, 9. doi: 10.1007/s11214-018-0576-4

Angelopoulos, V., Sibeck, D., Carlson, C. W., McFadden, J. P., Larson, D., Lin, R. P., ... Sigwarth, J. (2008, December). First Results from the THEMIS Mission. *Space Sci. Rev.*, *141*, 453-476. doi: 10.1007/s11214-008-9378-4

Angelopoulos, V., Zhang, X. J., Artemyev, A. V., Mourenas, D., Tsai, E., Wilkins, C., ... Zarifian, A. (2023, August). Energetic Electron Precipitation Driven by Electromagnetic Ion Cyclotron Waves from ELFIN's Low Altitude Perspective. *Space Sci. Rev.*, *219*(5), 37. doi: 10.1007/s11214-023-00984-w

Auster, H. U., Glassmeier, K. H., Magnes, W., Aydogar, O., Baumjohann, W., Constantinescu, D., ... Wiedemann, M. (2008, December). The THEMIS Fluxgate Magnetometer. *Space Sci. Rev.*, *141*, 235-264. doi: 10.1007/s11214-008-9365-9

Balikhin, M. A., Sagdeev, R. Z., Walker, S. N., Pokhotelov, O. A., Sibeck, D. G., Beloff, N., & Dudnikova, G. (2009, February). THEMIS observations of mirror structures: Magnetic holes and instability threshold. *Geophys. Res. Lett.*, *36*, 3105. doi: 10.1029/2008GL036923

Bashir, M. F., Artemyev, A., Zhang, X.-J., & Angelopoulos, V. (2022). Hot plasma effects on electron resonant scattering by electromagnetic ion cyclotron waves. *Geophysical Research Letters*, *49*(11), e2022GL099229. Retrieved from https://agupubs.onlinelibrary.wiley.com/doi/abs/10.1029/2022GL099229 (e2022GL099229 2022GL099229) doi: https://doi.org/10.1029/2022GL099229

Bashir, M. F., Artemyev, A., Zhang, X.-J., & Angelopoulos, V. (2022, June). Hot Plasma Effects on Electron Resonant Scattering by Electromagnetic Ion Cyclotron Waves. *Geophys. Res. Lett.*, *49*(11), e99229. doi: 10.1029/2022GL099229

Berchem, J., Fuselier, S. A., Petrinec, S., Frey, H. U., & Burch, J. L. (2003, October). Dayside Proton Aurora: Comparisons between Global MHD Simulations and IMAGE Observations. *Space Sci. Rev.*, *109*(1), 313-349. doi: 10.1023/B:SPAC.0000007523.23002.92

Blum, L. W., Agapitov, O., Bonnell, J. W., Kletzing, C., & Wygant, J. (2016, May). EMIC wave spatial and coherence scales as determined from multipoint Van Allen Probe measurements. *Geophys. Res. Lett.*, *43*, 4799-4807. doi: 10.1002/2016GL068799

Blum, L. W., Bonnell, J. W., Agapitov, O., Paulson, K., & Kletzing, C. (2017, February). EMIC wave scale size in the inner magnetosphere: Observations from the dual Van Allen Probes. *Geophys. Res. Lett.*, *44*, 1227-1233. doi: 10.1002/2016GL072316

Blum, L. W., Halford, A., Millan, R., Bonnell, J. W., Goldstein, J., Usanova, M., ... Li, X. (2015, July). Observations of coincident EMIC wave activity and duskside energetic electron precipitation on 18-19 January 2013. *Geophys. Res. Lett.*, *42*, 5727-5735. doi: 10.1002/2015GL065245

Bonnell, J. W., Mozer, F. S., Delory, G. T., Hull, A. J., Ergun, R. E., Cully, C. M., ... Harvey, P. R. (2008, December). The Electric Field Instrument (EFI) for THEMIS. *Space Sci. Rev.*, *141*, 303-341. doi: 10.1007/s11214-008-9469-2

Capannolo, L., Li, W., Ma, Q., Chen, L., Shen, X. C., Spence, H. E., ... Redmon, R. J. (2019, November). Direct Observation of Subrelativistic Electron Precipitation Potentially Driven by EMIC Waves. *Geophys. Res. Lett.*, *46*(22), 12,711-12,721. doi: 10.1029/2019GL084202

Capannolo, L., Li, W., Ma, Q., Qin, M., Shen, X.-C., Angelopoulos, V., ... Hanzelka, M. (2023, September). Electron Precipitation Observed by ELFIN Using Proton Precipitation as a Proxy for Electromagnetic Ion Cyclotron (EMIC) Waves. *arXiv e-prints*, arXiv:2309.07539. doi: 10.48550/arXiv.2309.07539

Capannolo, L., Li, W., Millan, R., Smith, D., Sivadas, N., Sample, J., & Shekhar, S. (2022, January). Relativistic Electron Precipitation Near Midnight: Drivers, Distribution, and Properties. *Journal of Geophysical Research (Space Physics)*, *127*(1), e30111. doi: 10.1029/2021JA030111

Chen, H., Gao, X., Lu, Q., & Wang, S. (2019, September). Analyzing EMIC Waves in the Inner Magnetosphere Using Long-Term Van Allen Probes Observations. *Journal of Geophysical Research (Space Physics)*, *124*(9), 7402-7412. doi: 10.1029/2019JA026965

Chen, L., Thorne, R. M., Jordanova, V. K., Wang, C.-P., Gkioulidou, M., Lyons, L., & Horne, R. B. (2010, Jul). Global simulation of EMIC wave excitation during the 21 April 2001 storm from coupled RCM-RAM-HOTRAY modeling. *Journal of Geophysical Research (Space Physics)*, *115*(A7), A07209. doi: 10.1029/2009JA015075

Cooper, M. B., Gerrard, A. J., Lanzerotti, L. J., Soto-Chavez, A. R., Kim, H., Kuzichev, I. V., & Goodwin, L. V. (2021, February). Mirror Instabilities in the Inner Magnetosphere and Their Potential for Localized ULF Wave Generation. *Journal of Geophysical Research (Space Physics)*, *126*(2), e28773. doi: 10.1029/2020JA028773

Drozdov, A. Y., Allison, H. J., Shprits, Y. Y., Usanova, M. E., Saikin, A., & Wang, D. (2022, April). Depletions of Multi-MeV Electrons and Their Association to Minima in Phase Space Density. *Geophys. Res. Lett.*, *49*(8), e97620. doi: 10.1029/2021GL097620

Frey, H. U. (2007, March). Localized aurora beyond the auroral oval. *Reviews of Geophysics*, *45*(1), RG1003. doi: 10.1029/2005RG000174

Fu, S., Ni, B., Lou, Y., Bortnik, J., Ge, Y., Tao, X., . . . Wang, Q. (2018, October). Resonant Scattering of Near-Equatorially Mirroring Electrons by Landau Resonance With H^+ Band EMIC Waves. *Geophys. Res. Lett.*, *45*(20), 10,866-10,873. doi: 10.1029/2018GL079718

Gamayunov, K. V., & Engebretson, M. J. (2021, August). Low Frequency ULF Waves in the Earth's Inner Magnetosphere: Statistics During Coronal Mass Ejections and Seeding of EMIC Waves. *Journal of Geophysical Research (Space Physics)*, *126*(8), e29247. doi: 10.1029/2021JA029247

Gamayunov, K. V., & Engebretson, M. J. (2022, November). Low Frequency ULF Waves in the Earth's Inner Magnetosphere: Power Spectra During High Speed Streams and Quiet Solar Wind and Seeding of EMIC Waves. *Journal of Geophysical Research (Space Physics)*, *127*(11), e2022JA030647. doi: 10.1029/2022JA030647

Gamayunov, K. V., Engebretson, M. J., & Elkington, S. R. (2020, September). EMIC Waves in the Earth's Inner Magnetosphere as a Function of Solar Wind Structures During Solar Maximum. *Journal of Geophysical Research (Space Physics)*, *125*(9), e27990. doi: 10.1029/2020JA027990

Gamayunov, K. V., & Khazanov, G. V. (2007, July). Effect of oblique electromagnetic ion cyclotron waves on relativistic electron scattering: Combined Release and Radiation Effects Satellite (CRRES)-based calculation. *Journal of Geophysical Research (Space Physics)*, *112*(A7), A07220. doi: 10.1029/2007JA012300

Halford, A. J., Fraser, B. J., & Morley, S. K. (2015, March). EMIC waves and plasmaspheric and plume density: CRRES results. *Journal of Geophysical Research (Space Physics)*, *120*(3), 1974-1992. doi: 10.1002/2014JA020338

Hartinger, M., Angelopoulos, V., Moldwin, M. B., Glassmeier, K.-H., & Nishimura, Y. (2011, Jun). Global energy transfer during a magnetospheric field line resonance. *Geophys. Res. Lett.*, *38*(12), L12101. doi: 10.1029/2011GL047846

Hartinger, M. D., Turner, D. L., Plaschke, F., Angelopoulos, V., & Singer, H. (2013, January). The role of transient ion foreshock phenomena in driving Pc5 ULF wave activity. *J. Geophys. Res.*, *118*, 299-312. doi: 10.1029/2012JA018349

Hartinger, M. D., Welling, D., Viall, N. M., Moldwin, M. B., & Ridley, A. (2014, October). The effect of magnetopause motion on fast mode resonance. *J. Geophys. Res.*, *119*, 8212-8227. doi: 10.1002/2014JA020401

Hasegawa, A. (1969). Drift mirror instability of the magnetosphere. *Physics of Fluids*, *12*, 2642-2650. doi: 10.1063/1.1692407

Inaba, Y., Shiokawa, K., Oyama, S.-i., Otsuka, Y., Connors, M., Schofield, I., . . . Bonnell, J. W. (2021, April). Multi Event Analysis of Plasma and Field Variations in Source of Stable Auroral Red (SAR) Arcs in Inner Magnetosphere During Non Storm Time Substorms. *Journal of Geophysical Research (Space Physics)*, *126*(4), e29081. doi: 10.1029/2020JA029081

Jordanova, V. K., Farrugia, C. J., Thorne, R. M., Khazanov, G. V., Reeves, G. D., & Thomsen, M. F. (2001, January). Modeling ring current proton precipitation by electromagnetic ion cyclotron waves during the May 14-16, 1997, storm. *J. Geophys. Res.*, *106*, 7-22. doi: 10.1029/2000JA002008

Jordanova, V. K., Spasojevic, M., & Thomsen, M. F. (2007, August). Modeling the electromagnetic ion cyclotron wave-induced formation of detached subauroral proton arcs. *J. Geophys. Res.*, *112*, A08209. doi: 10.1029/2006JA012215

Jun, C.-W., Miyoshi, Y., Kurita, S., Yue, C., Bortnik, J., Lyons, L., . . . Shinohara,

I. (2021, June). The Characteristics of EMIC Waves in the Magnetosphere Based on the Van Allen Probes and Arase Observations. *Journal of Geophysical Research (Space Physics)*, *126*(6), e29001. doi: 10.1029/2020JA029001

Jun, C. W., Yue, C., Bortnik, J., Lyons, L. R., Nishimura, Y., & Kletzing, C. (2019, Mar). EMIC Wave Properties Associated With and Without Injections in The Inner Magnetosphere. *Journal of Geophysical Research (Space Physics)*, *124*(3), 2029-2045. doi: 10.1029/2018JA026279

Kennel, C. F. (1969). Consequences of a magnetospheric plasma. *Reviews of Geophysics and Space Physics*, *7*, 379-419. doi: 10.1029/RG007i001p00379

Kennel, C. F., & Petschek, H. E. (1966, January). Limit on Stably Trapped Particle Fluxes. *J. Geophys. Res.*, *71*, 1-28.

Kersten, T., Horne, R. B., Glauert, S. A., Meredith, N. P., Fraser, B. J., & Grew, R. S. (2014, November). Electron losses from the radiation belts caused by EMIC waves. *J. Geophys. Res.*, *119*, 8820-8837. doi: 10.1002/2014JA020366

Khazanov, G. V., & Gamayunov, K. V. (2007, October). Effect of electromagnetic ion cyclotron wave normal angle distribution on relativistic electron scattering in outer radiation belt. *Journal of Geophysical Research (Space Physics)*, *112*(A10), A10209. doi: 10.1029/2007JA012282

Khazanov, G. V., Gamayunov, K. V., Gallagher, D. L., Kozyra, J. U., & Liemohn, M. W. (2007, April). Self-consistent model of magnetospheric ring current and propagating electromagnetic ion cyclotron waves: 2. Wave-induced ring current precipitation and thermal electron heating. *J. Geophys. Res.*, *112*, A04209. doi: 10.1029/2006JA012033

Kitamura, N., Kitahara, M., Shoji, M., Miyoshi, Y., Hasegawa, H., Nakamura, S., ... Burch, J. L. (2018, September). Direct measurements of two-way wave-particle energy transfer in a collisionless space plasma. *Science*, *361*(6406), 1000-1003. doi: 10.1126/science.aap8730

Kitamura, N., Shoji, M., Nakamura, S., Kitahara, M., Amano, T., Omura, Y., ... Burch, J. L. (2021, May). Energy Transfer Between Hot Protons and Electromagnetic Ion Cyclotron Waves in Compressional Pc5 Ultra low Frequency Waves. *Journal of Geophysical Research (Space Physics)*, *126*(5), e28912. doi: 10.1029/2020JA028912

Liu, N., Jin, Y., He, Z., Yu, J., Li, K., & Cui, J. (2022, May). Simultaneous Evolutions of Inner Magnetospheric Plasmaspheric Hiss and EMIC Waves Under the Influence of a Heliospheric Plasma Sheet. *Geophys. Res. Lett.*, *49*(10), e98798. doi: 10.1029/2022GL098798

Liu, Z. Y., Zong, Q. G., Rankin, R., Zhang, H., Wang, Y. F., Zhou, X. Z., ... Le, G. (2022, September). Simultaneous macroscale and microscale wave-ion interaction in near-earth space plasmas. *Nature Communications*, *13*, 5593. doi: 10.1038/s41467-022-33298-6

Lorentzen, D. A., & Moen, J. (2000, June). Auroral proton and electron signatures in the dayside aurora. *J. Geophys. Res.*, *105*(A6), 12733-12746. doi: 10.1029/1999JA900405

Loto'Aniu, T. M., Fraser, B. J., & Waters, C. L. (2009, January). The modulation of electromagnetic ion cyclotron waves by Pc 5 ULF waves. *Annales Geophysicae*, *27*(1), 121-130. doi: 10.5194/angeo-27-121-2009

Ma, Q., Li, W., Thorne, R. M., Ni, B., Kletzing, C. A., Kurth, W. S., ... Angelopoulos, V. (2015, February). Modeling inward diffusion and slow decay of energetic electrons in the Earth's outer radiation belt. *Geophys. Res. Lett.*, *42*, 987-995. doi: 10.1002/2014GL062977

Ma, Q., Li, W., Yue, C., Thorne, R. M., Bortnik, J., Kletzing, C. A., ... Spence, H. E. (2019, June). Ion Heating by Electromagnetic Ion Cyclotron Waves and Magnetosonic Waves in the Earth's Inner Magnetosphere. *Geophys. Res. Lett.*, *46*(12), 6258-6267. doi: 10.1029/2019GL083513

McFadden, J. P., Carlson, C. W., Larson, D., Ludlam, M., Abiad, R., Elliott, B.,

. . . Angelopoulos, V. (2008, December). The THEMIS ESA Plasma Instrument and In-flight Calibration. *Space Sci. Rev.*, *141*, 277-302. doi: 10.1007/s11214-008-9440-2

Millan, R. M., & Thorne, R. M. (2007, March). Review of radiation belt relativistic electron losses. *Journal of Atmospheric and Solar-Terrestrial Physics*, *69*, 362-377. doi: 10.1016/j.jastp.2006.06.019

Nishimura, Y., Bortnik, J., Li, W., Thorne, R. M., Ni, B., Lyons, L. R., . . . Auster, U. (2013, Feb). Structures of dayside whistler-mode waves deduced from conjugate diffuse aurora. *Journal of Geophysical Research (Space Physics)*, *118*(2), 664-673. doi: 10.1029/2012JA018242

Rae, I. J., Mann, I. R., Watt, C. E. J., Kistler, L. M., & Baumjohann, W. (2007, November). Equator-S observations of drift mirror mode waves in the dawnside magnetosphere. *Journal of Geophysical Research (Space Physics)*, *112*(A11), A11203. doi: 10.1029/2006JA012064

Ross, J. P. J., Glauert, S. A., Horne, R. B., Watt, C. E. J., & Meredith, N. P. (2021, December). On the Variability of EMIC Waves and the Consequences for the Relativistic Electron Radiation Belt Population. *Journal of Geophysical Research (Space Physics)*, *126*(12), e29754. doi: 10.1029/2021JA029754

Shumko, M., Gallardo-Lacourt, B., Halford, A. J., Blum, L. W., Liang, J., Miyoshi, Y., . . . Gillies, D. M. (2022, August). Proton aurora and relativistic electron microbursts scattered by electromagnetic ion cyclotron waves. *Frontiers in Astronomy and Space Sciences*, *9*, 975123. doi: 10.3389/fspas.2022.975123

Sigernes, F., Fasel, L. G., Minow, J., Deehr, C. S., Smith, R. W., Lorentzen, D. A., . . . Henriksen, K. (1996, August). Calculations and ground-based observations of pulsed proton events in the dayside aurora. *Journal of Atmospheric and Terrestrial Physics*, *58*(11), 1281-1291. doi: 10.1016/0021-9169(95)00113-1

Soto-Chavez, A. R., Lanzerotti, L. J., Manweiler, J. W., Gerrard, A., Cohen, R., Xia, Z., . . . Kim, H. (2019, April). Observational evidence of the drift-mirror plasma instability in Earth's inner magnetosphere. *Physics of Plasmas*, *26*(4), 042110. doi: 10.1063/1.5083629

Stix, T. H. (1962). *The Theory of Plasma Waves.*

Summers, D., Ni, B., & Meredith, N. P. (2007, April). Timescales for radiation belt electron acceleration and loss due to resonant wave-particle interactions: 2. Evaluation for VLF chorus, ELF hiss, and electromagnetic ion cyclotron waves. *J. Geophys. Res.*, *112*, 4207. doi: 10.1029/2006JA011993

Summers, D., & Thorne, R. M. (2003, April). Relativistic electron pitch-angle scattering by electromagnetic ion cyclotron waves during geomagnetic storms. *J. Geophys. Res.*, *108*, 1143. doi: 10.1029/2002JA009489

Usanova, M. E. (2021, September). Energy Exchange Between Electromagnetic Ion Cyclotron (EMIC) Waves and Thermal Plasma: From Theory to Observations. *Frontiers in Astronomy and Space Sciences*, *8*, 150. doi: 10.3389/fspas.2021.744344

Usanova, M. E., Darrouzet, F., Mann, I. R., & Bortnik, J. (2013, August). Statistical analysis of EMIC waves in plasmaspheric plumes from Cluster observations. *Journal of Geophysical Research (Space Physics)*, *118*(8), 4946-4951. doi: 10.1002/jgra.50464

Usanova, M. E., Drozdov, A., Orlova, K., Mann, I. R., Shprits, Y., Robertson, M. T., . . . Wygant, J. (2014, March). Effect of EMIC waves on relativistic and ultrarelativistic electron populations: Ground-based and Van Allen Probes observations. *Geophys. Res. Lett.*, *41*, 1375-1381. doi: 10.1002/2013GL059024

Usanova, M. E., Mann, I. R., Bortnik, J., Shao, L., & Angelopoulos, V. (2012, October). THEMIS observations of electromagnetic ion cyclotron wave occurrence: Dependence on AE, SYMH, and solar wind dynamic pressure. *J. Geophys. Res.*, *117*, 10218. doi: 10.1029/2012JA018049

Wang, B., Li, P., Huang, J., & Zhang, B. (2019, April). Nonlinear Landau resonance between EMIC waves and cold electrons in the inner magnetosphere. *Physics of Plasmas*, *26*(4), 042903. doi: 10.1063/1.5088374

Wang, B., Nishimura, Y., Hietala, H., Lyons, L., Angelopoulos, V., Plaschke, F., . . . Weatherwax, A. (2018, Jun). Impacts of Magnetosheath High-Speed Jets on the Magnetosphere and Ionosphere Measured by Optical Imaging and Satellite Observations. *Journal of Geophysical Research*, *123*(6), 4879-4894. doi: 10.1029/2017JA024954

Wang, B., Nishimura, Y., Zhang, H., Shen, X.-C., Lyons, L., Angelopoulos, V., . . . Frey, H. U. (2019, Aug). The 2-D Structure of Foreshock-Driven Field Line Resonances Observed by THEMIS Satellite and Ground-Based Imager Conjunctions. *Journal of Geophysical Research (Space Physics)*, *124*(8), 6792-6811. doi: 10.1029/2019JA026668

Xue, Z., Yuan, Z., Yu, X., Deng, D., Huang, Z., & Raita, T. (2022, May). EMIC Waves Observed Throughout the Inner Magnetosphere Driven by Abrupt Enhancement of the Solar Wind Pressure. *Geophys. Res. Lett.*, *49*(9), e98954. doi: 10.1029/2022GL098954

Yahnin, A. G., Yahnina, T. A., Raita, T., & Manninen, J. (2017, September). Ground pulsation magnetometer observations conjugated with relativistic electron precipitation. *Journal of Geophysical Research (Space Physics)*, *122*(9), 9169-9182. doi: 10.1002/2017JA024249

Yahnin, A. G., Yahnina, T. A., Semenova, N. V., Gvozdevsky, B. B., & Pashin, A. B. (2016, September). Relativistic electron precipitation as seen by NOAA POES. *Journal of Geophysical Research (Space Physics)*, *121*(9), 8286-8299. doi: 10.1002/2016JA022765

Yin, Z.-F., Zhou, X.-Z., Hu, Z.-J., Yue, C., Zong, Q.-G., Hao, Y.-X., . . . Manweiler, J. W. (2022, June). Localized Excitation of Electromagnetic Ion Cyclotron Waves From Anisotropic Protons Filtered by Magnetic Dips. *Journal of Geophysical Research (Space Physics)*, *127*(6), e30531. doi: 10.1029/2022JA030531

Zhang, X.-J., Li, W., Thorne, R. M., Angelopoulos, V., Bortnik, J., Kletzing, C. A., . . . Hospodarsky, G. B. (2016, December). Statistical distribution of EMIC wave spectra: Observations from Van Allen Probes. *Geophys. Res. Lett.*, *43*, 12. doi: 10.1002/2016GL071158

Figure 1.

a
b
c
d
e
f
g
h
B [nT GSM]
bz
by
bx
f_{pe}/f_{ce}
scpot
ESA
dBII(nT)
E(eV)
EFlux
PAD (deg)
F(Hz)
nT^2/Hz
Ellip
WNA
L
MLT
LAT
hhmm
7.8 8.4
13.7 13.9
-2.3 -3.0
2230 2300
2017 Jun 22
8.3 7.6 7.0
11.9 12.1 12.3
-3.2 -2.3 -1.5
0800 0830 0900
2017 Oct 12
7.6 8.2 8.9 9.5
11.5 11.7 11.9 12.0
2.7 3.6 4.6 5.6
1000 1030 1100 1130
2018 Sep 14

Figure 2.

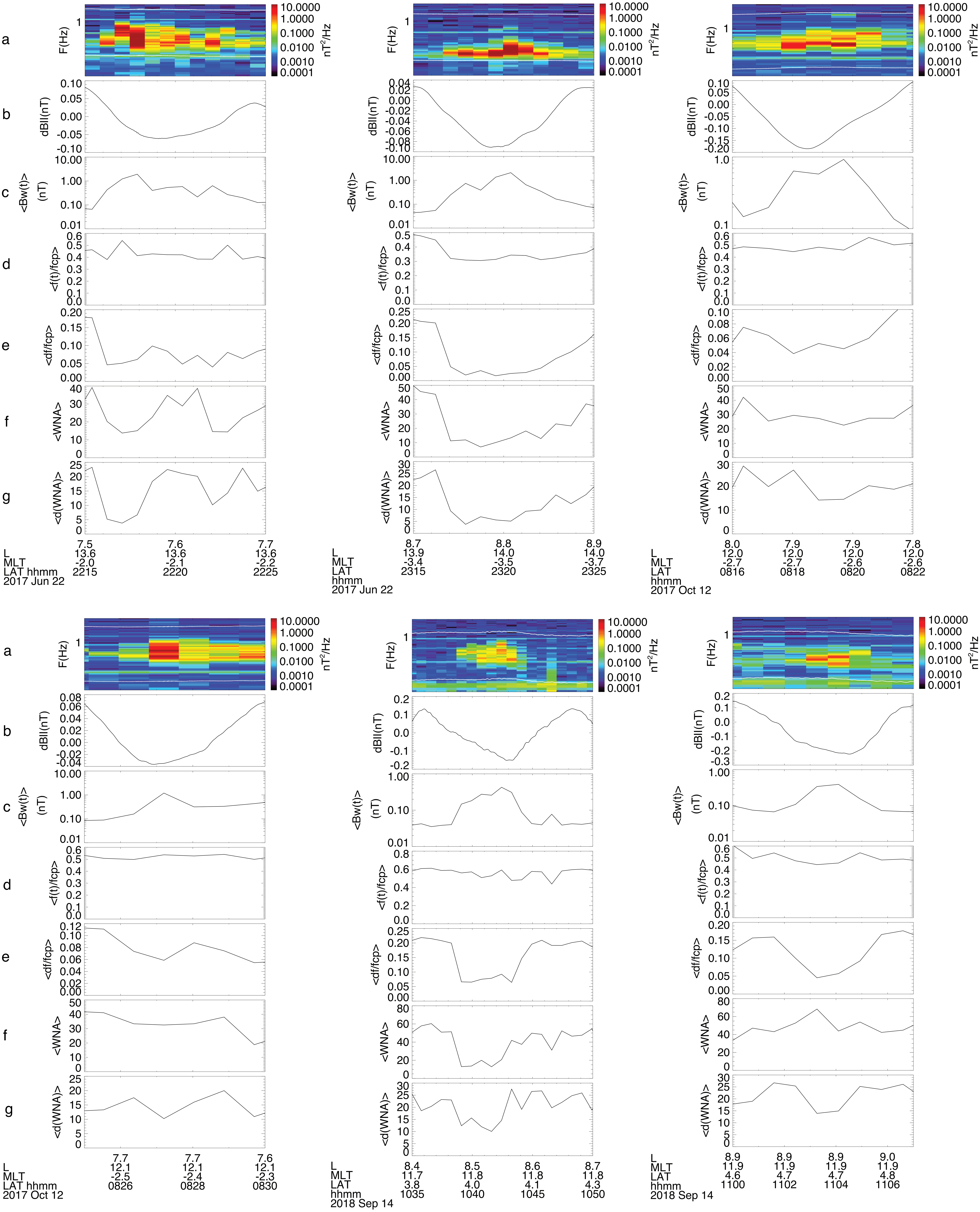
a
F(Hz)
10.0000
1.0000
0.1000
0.0100
0.0010
0.0001
nT²/Hz
b
dBll(nT)
c
<Bw(t)>
(nT)
d
<f(t)/fcp>
e
<df/fcp>
f
<WNA>
g
<d(WNA)>
L 7.5 7.6 7.7
MLT 13.6 13.6 13.6
LAT -2.0 -2.1 -2.2
hhmm 2215 2220 2225
2017 Jun 22
L 8.7 8.8 8.9
MLT 13.9 14.0 14.0
LAT -3.4 -3.5 -3.7
hhmm 2315 2320 2325
2017 Jun 22
L 8.0 7.9 7.9 7.8
MLT 12.0 12.0 12.0 12.0
LAT -2.7 -2.7 -2.6 -2.6
hhmm 0816 0818 0820 0822
2017 Oct 12
L 7.7 7.7 7.6
MLT 12.1 12.1 12.1
LAT -2.5 -2.4 -2.3
hhmm 0826 0828 0830
2017 Oct 12
L 8.4 8.5 8.6 8.7
MLT 11.7 11.8 11.8 11.8
LAT 3.8 4.0 4.1 4.3
hhmm 1035 1040 1045 1050
2018 Sep 14
L 8.9 8.9 8.9 9.0
MLT 11.9 11.9 11.9 11.9
LAT 4.6 4.7 4.7 4.8
hhmm 1100 1102 1104 1106
2018 Sep 14

Figure 3.

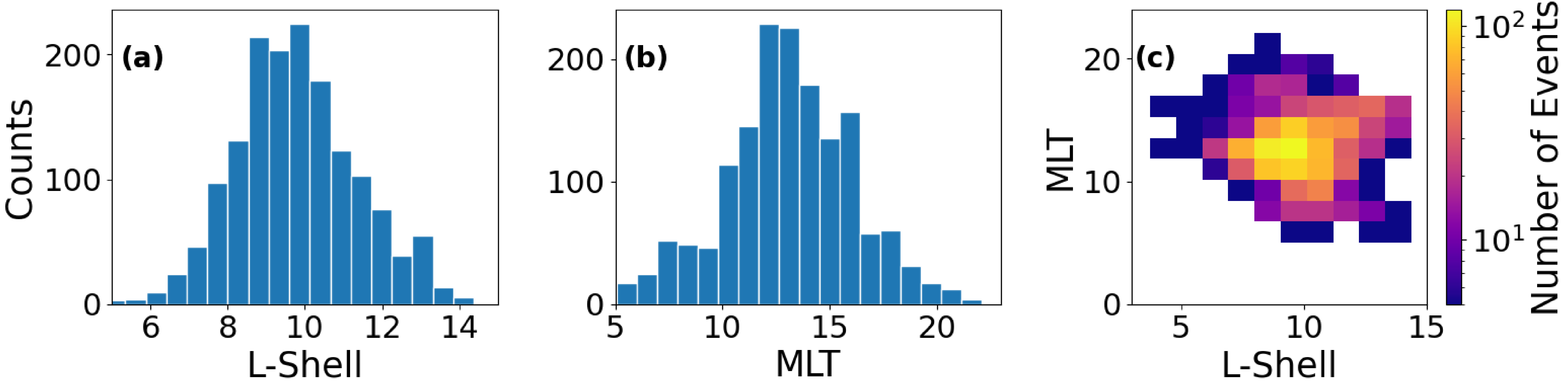

(a)
Counts
L-Shell
0
100
200
6
8
10
12
14
(b)
MLT
0
100
200
5
10
15
20
(c)
MLT
L-Shell
0
10
20
5
10
15
Number of Events
10^2
10^1

Figure 4.

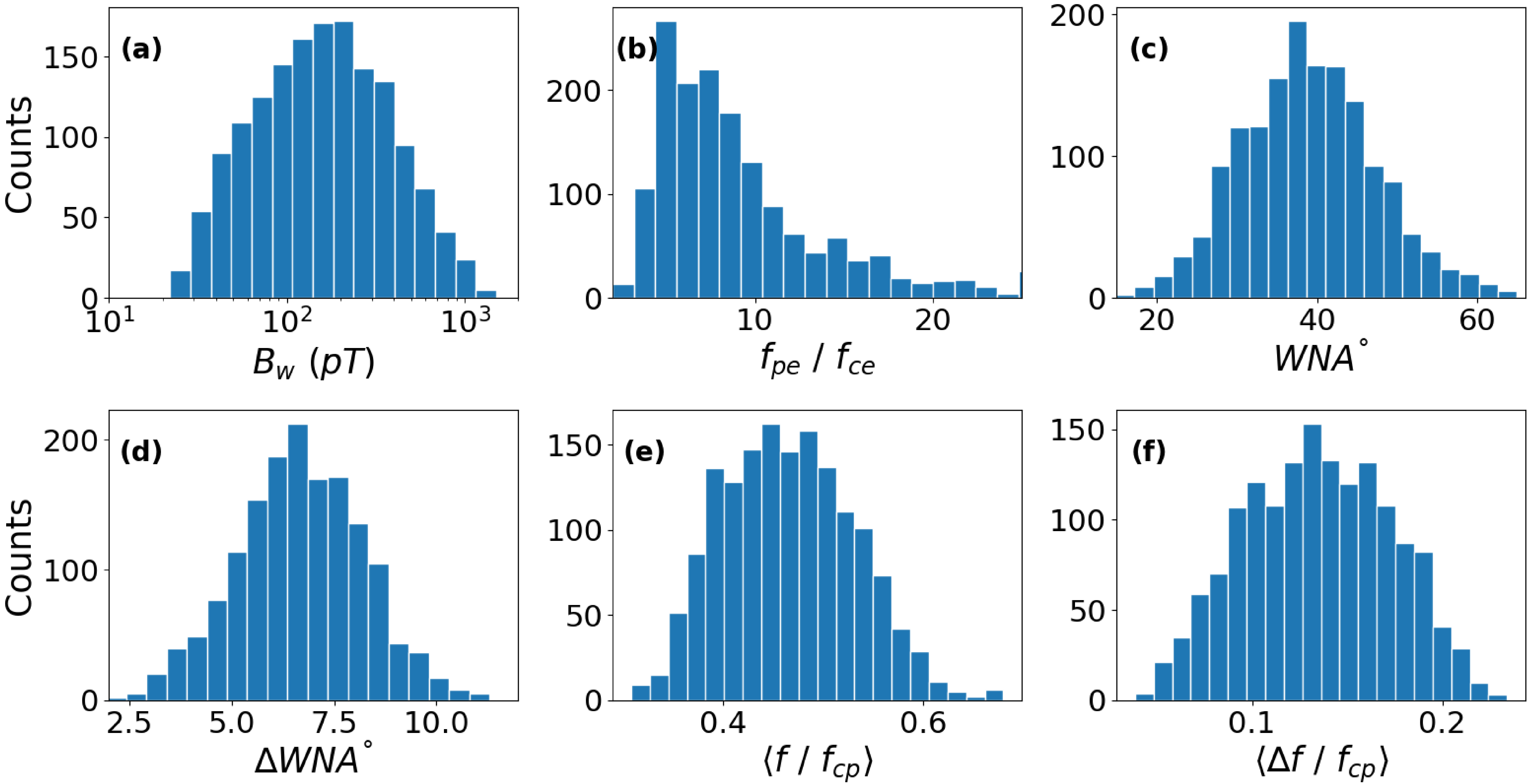

(a)
Counts
0
50
100
150
10^1
10^2
10^3
B_w (pT)
(b)
0
100
200
10
20
f_{pe} / f_{ce}
(c)
0
100
200
20
40
60
WNA°
(d)
Counts
0
100
200
2.5
5.0
7.5
10.0
ΔWNA°
(e)
0
50
100
150
0.4
0.6
$\langle f / f_{cp} \rangle$
(f)
0
50
100
150
0.1
0.2
$\langle \Delta f / f_{cp} \rangle$

Figure 5.

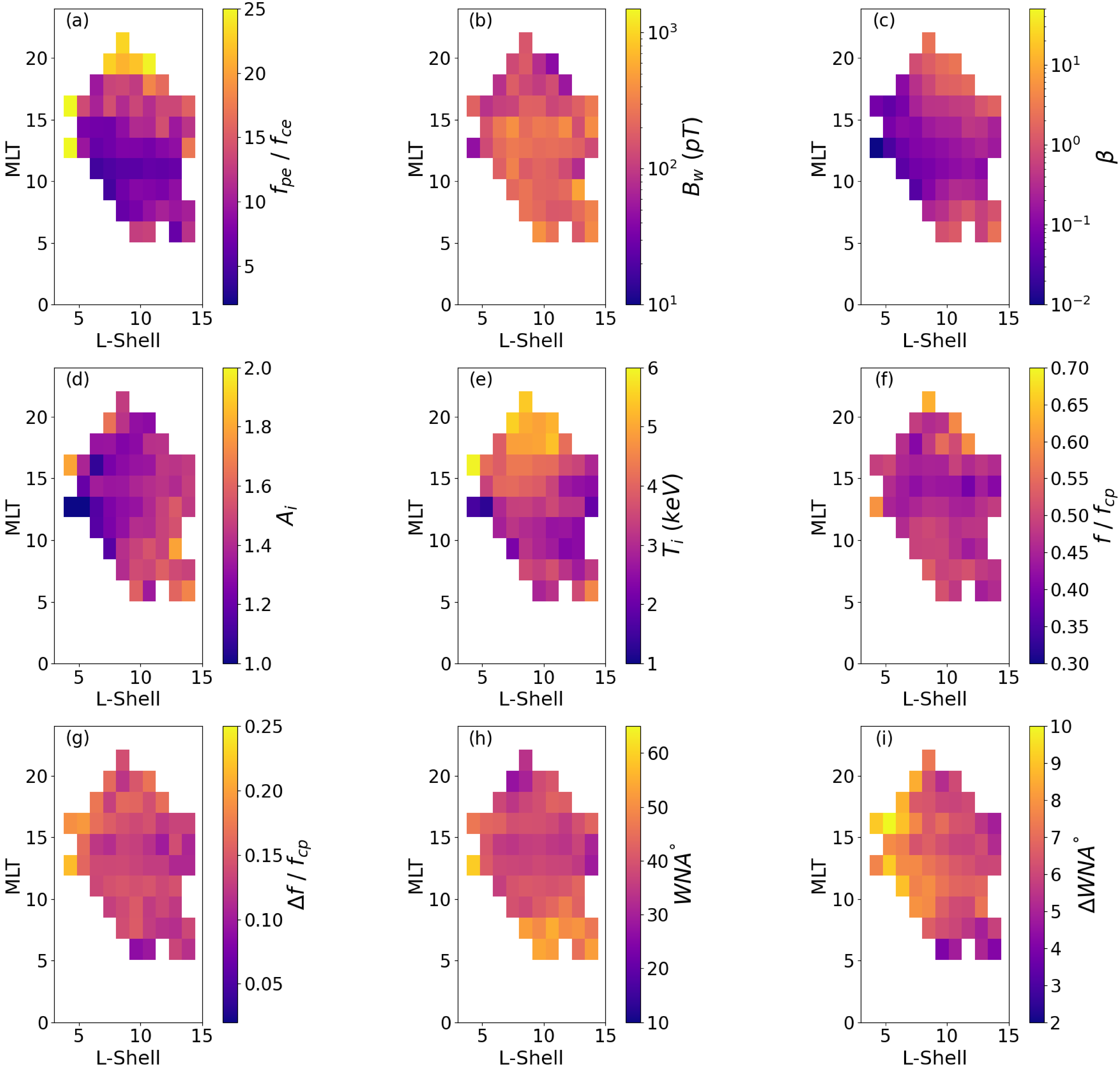

(a)
(b)
(c)
(d)
(e)
(f)
(g)
(h)
(i)
MLT
L-Shell
f_{pe} / f_{ce}
B_w (pT)
β
A_i
T_i (keV)
f / f_{cp}
Δf / f_{cp}
WNA°
ΔWNA°

Figure 6.

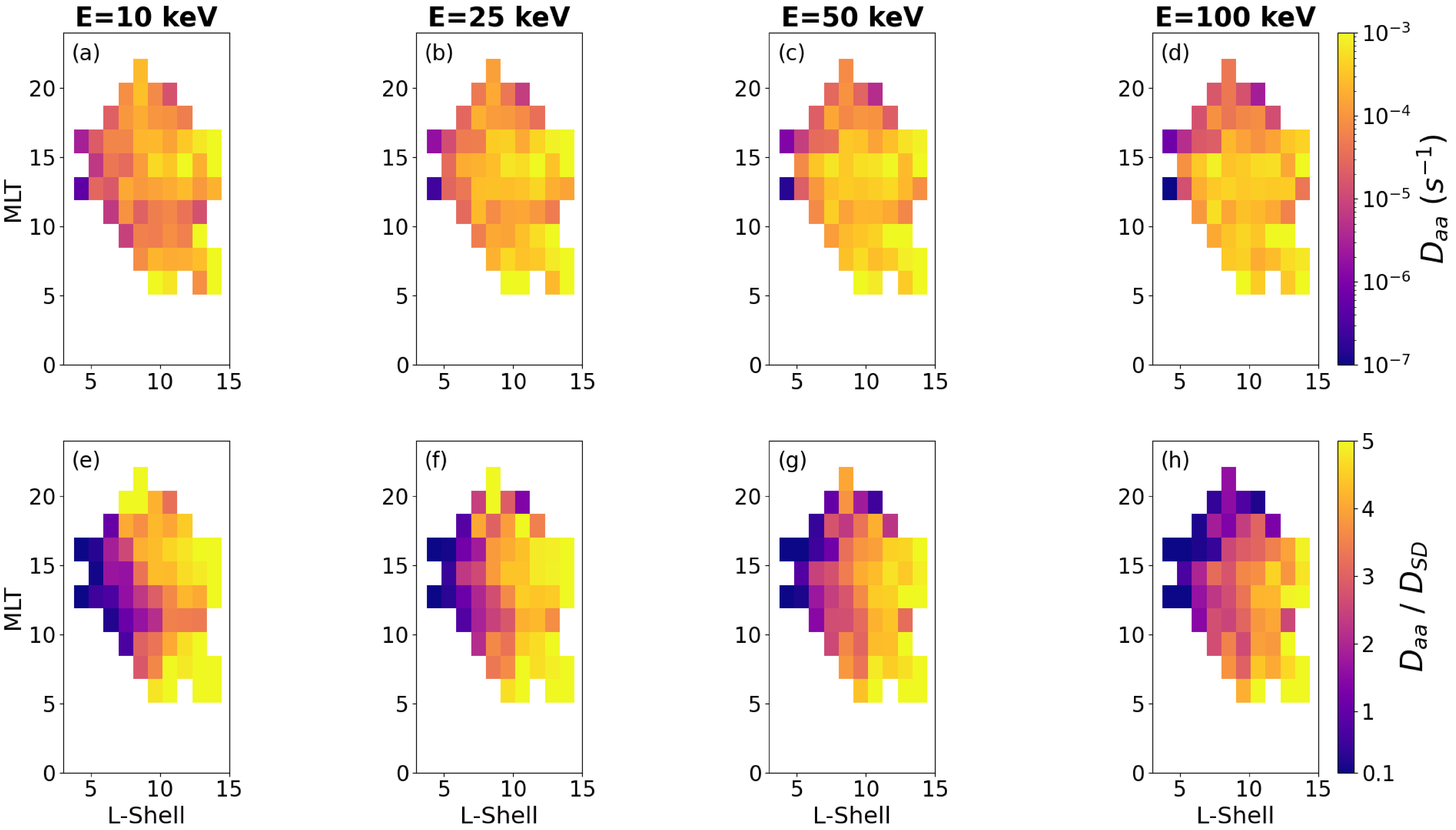
E=10 keV
E=25 keV
E=50 keV
E=100 keV
(a)
(b)
(c)
(d)
(e)
(f)
(g)
(h)
MLT
L-Shell
D_{aa} (s^{-1})
D_{aa} / D_{SD}
10^{-3}
10^{-4}
10^{-5}
10^{-6}
10^{-7}
5
4
3
2
1
0.1